JMEPEG (2011) 20:1467–1473
DOI: 10.1007/s11665-010-9782-2

1059-9495/$19.00

# The Optimization of Interlamellar Spacing in a Nanopearlitic Lead-Patented Hypoeutectoid Steel Wire

*J. Aghazadeh Mohandesi and M. Saadatmand*

*(Submitted February 14, 2010; in revised form September 21, 2010)*

**In this study, in order to optimize the interlamellar spacing prior to drawing operation in a nanopearlitic lead patented hypoeutectoid steel wire, a model based on finite element method is presented to predict the optimum immersion time in a lead bath. A typical suitable immersion time for the wire with 1.8 mm diameter is about 10 s. The austenitizing and quenching temperature for a wire with diameter of 1.8 mm and composition of 0.72% C, to obtain the lowest interlamellar spacing (i.e., 29 nm), are 910 and 510 °C, respectively. The hardness and the yield strength of the steel wire followed a linear relationship with the inverse square root of the interlamellar spacing ($S^{-1/2}$). Pearlite interlamellar spacing obtained after patenting treatment, was decreased by increasing the amount of prior deformation.**

**Keywords** atomic force microscopy, finite element method, interlamellar spacing, nanopearlitic patented steel

## 1. Introduction

A little over 100 years ago, wire rod was rolled on hand-fed three-high mills in straight lengths of about 14 ft by 1/2 in. diameter. The looping mill had not yet been invented. High carbon rod was rolled from wrought iron which had been carbonized by ''cementation''. In this process, bars were heated to a red hot condition for a week in contact with charcoal in firebrick pots luted with grindstone wheel swarf to exclude the air (Ref 1). The bars were reheated and hammered and then rolled into rods which were drawn into wire to produce such products as piano wire. The cemented rod was very difficult to draw because of its hardness and brittleness. Then, in 1854, James Horsfall of Hay Mills, Birmingham, England, patented a process for heat treating the rod and wire to make it easier to draw (Ref 2). At that time, this process must have had a great impact upon the industry because the heat treatment is called ''patenting'' even to this day (Ref 1). The objective of patenting is to obtain a structure which combines high tensile strength with high ductility, and thus enable the wire to withstand a large reduction in area to produce the desired finished sizes possessing a combination of high tensile strength and good toughness (Ref 3). Patenting is normally conducted as a continuous process and typically consists of heating the alloy to form face centered cubic austenite, and then cooling at a rapid rate to a lower temperature at which transformation occurs to that of pearlite, an eutectoid mixture of based centered cubic ferrite and cementite, which yields the desired mechanical properties.

The wide range of mechanical properties of pearlitic microstructures, which made the ferritic-pearlitic steels by far the most consumed structural material in the world, is intrinsically related to the pearlite interlamellar spacing. It is, therefore, not surprising that it has been reported for decades the influence of the cooling conditions on the interlamellar spacing of pearlite (Ref 4, 5) as well as the role of the interlamellar spacing on the austenite formation during the isothermal and continuous heating of steels (Ref 6, 7). Thus, the study of the factors which influence the interlamellar spacing of pearlite formation remains an interesting topic.

The classical metallographic techniques, usually applied to the measurement of pearlite interlamellar spacing, were reviewed by Ridley (Ref 8) who pointed out that the examination of thin foil specimens or shadowed carbon replicas by transmission electron microscopy (TEM) is the most versatile technique employed to analyze fine pearlites. The parameter most frequently used to characterize the pearlitic structures is, according to Ridley, the minimum observed spacing, $S_{min}$, measured on the electron photomicrographs or on the fluorescent screen of the microscope. One method for measuring $S_{min}$ is to search for pearlite colonies of minimum spacing and to count the number of lamellae crossed at right angles by a diametric line of a scribed circle of known size on the fluorescent screen of the microscope. Another method involves similar measurements made on the TEM photomicrographs of known magnification (Ref 9). Both methods require skillful selection of the observation areas, particularly in the case of deformed pearlites. Another difficulty with these measurement methods is the preparation of the samples for TEM observation, which is not an easy task and requires a great deal of experience in selecting the preparation techniques suitable for a particular set of operating conditions of the electron microscope. The whole procedure is time consuming and has turned out to be of limited use for routine purposes.

**J. Aghazadeh Mohandesi,** and **M. Saadatmand**, Amirkabir University of Technology, Tehran, Iran. Contact e-mail: saadatmand83@yahoo.com.

Techniques usually applied in conventional optical microscopy, including the partial resolution method, are strongly limited by the resolving power of the optical microscopes and cannot be used in the measurement of the interlamellar spacing of fine or deformed pearlites (Ref 8).

High resolution, easy sample preparation together with easier operation of the atomic force microscopy as well as its lower cost, compared to transmission electron microscopy, makes it an attractive replacement for transmission electron microscopy in such studies. In this study, the atomic force microscopy (AFM) (Ref 10) has been applied to measure the pearlite interlamellar spacing in the lead patented steel wire.

In near eutectoid steels, the pearlite phase governs the strength, while the ferrite phase controls the ductility (Ref 11). It is clearly mentioned in the literature (Ref 12-14) that an increase in the volume fraction of the pearlite phase improves the flow stress of the ferritic-pearlitic steels. It has also been reported by several investigators (Ref 15, 16) that the strength of the ferrite follows a Hall-Petch type relationship with its grain size. Similarly, the strength of the pearlite phase has also been reported to follow a Hall-Petch type relationship with respect to the interlamellar spacing (Ref 17). Sevillano (Ref 18) and Ray and Mondal (Ref 19) have suggested that in eutectoid steels, the dependence of the strength of the pearlite on the interlamellar spacing eutectoid steel follows the Brown and Ham (Ref 20) equation.

For hypoeutectoid steels with coarse pearlite, the relation between interlamellar spacing and undercooling has been investigated (Ref 12, 21). The yield stress of high carbon steels is controlled by pearlite interlamellar spacing. For hypoeutectoid steel, there are different equations for describing the relation between yield stress and interlamellar spacing (Ref 18-20, 22, 23). The obtained results of this study verify these relations for nanostructure eutectoid steels. In addition to that, a few relations between the process parameters and nanostructure and mechanical properties are suggested for the hypoeutectoid steels with fine pearlite.

The aim of this investigation is to model the cooling rates in lead and air mediums by finite element method, to achieve nanopearlitic structure and a relationship between undercooling and interlamellar spacing, and to examine the effect of interlamellar spacing on the mechanical properties of 0.72% C nanopearlitic hypo-eutectoid steel.

## 2. Materials and Experimental Procedures

High carbon (0.72 wt.%) steel wire with 1.8-mm diameter was used (ASTM A228) as raw material. To model the air and lead patenting, the finite element method was used. In this method, by ABAQUS software, the heat transfer along transverse section of the wire was calculated. Data used for analysis are shown in Table. 1.

Metallographic preparation of the steel specimens involved mounting arrangement in Bakelite followed by manual grinding using successively finer silicon carbide papers from 60 to 1000 grit and fine polishing. To reveal the general microstructures of the isothermally transformed samples at different temperatures, the specimens were etched in 2% Nital and examined by scanning electron microscope (SEM) (Fig. 1) and AFM.

For achieving the nanopearlitic structure in the lead patenting, the quenching temperatures of 510, 525, 540, 555, and 570 °C, and austenitizing temperatures of 910, 930, 950, 970, and 990 °C were considered. Austenitizing time was 10 s for all the samples.

To measure the real interlamellar spacing, the colony with the lowest interlamellar spacing (i.e., with lamella perpendicular to the surface) in an area of 50 μm × 50 μm was selected for AFM analysis. A typical colony is shown in Fig. 2. To obtain the precise interlamellar spacing, the measurement was carried out in three different parts of the specimen: near the surface (A), beneath the surface (B), and middle of the wire (C) as shown in Fig. 3.

**Table 1 The data used for analysis by finite element**

| | Air | Lead |
|---|---|---|
| Wire temperature, °C | 900 | 900 |
| Medium temperature, °C | 25 | 500 |
| Convection coefficient, W/m$^2$ K | 10 | 2000 |

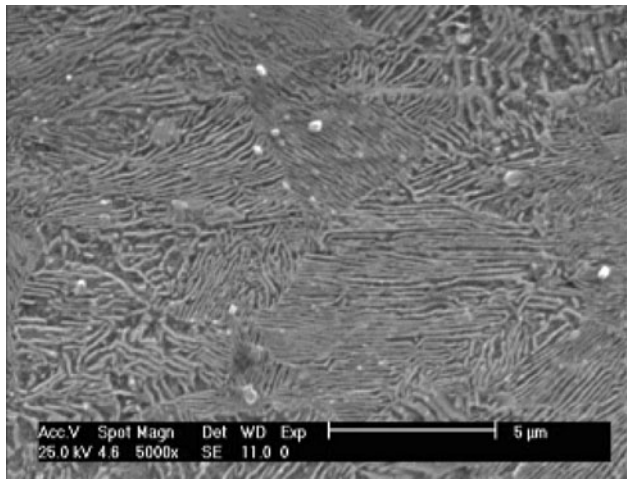


**Fig. 1** SEM micrographs of the colonies of pearlite for a typical sample of the patented steel

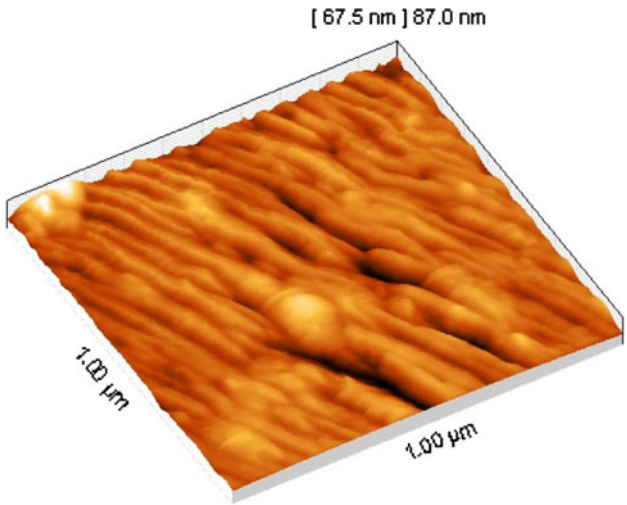


**Fig. 2** The topographic features on AFM image for a typical sample of the patented steel (scan speed: 10 μm/s, applied force: 3 nN)

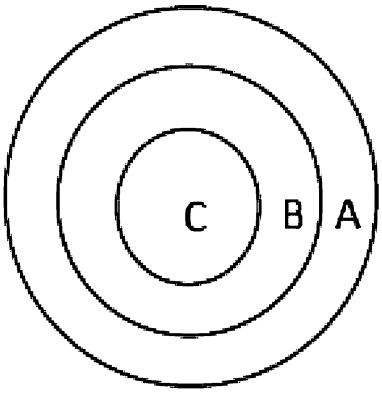


**Fig. 3** Different parts of sample to measure interlamellar spacing

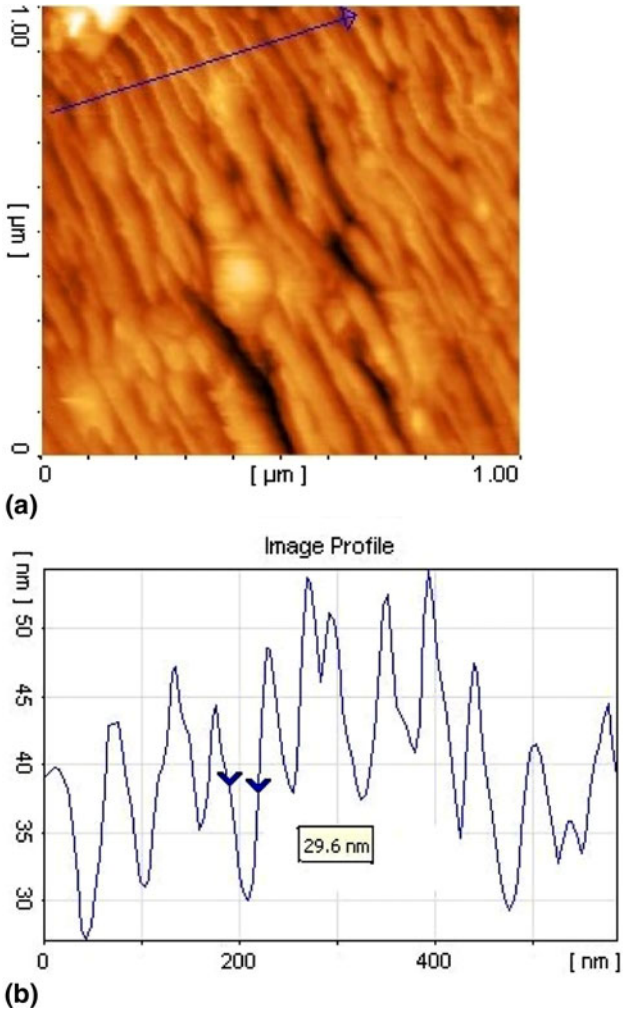


**Fig. 4** (a) Test-line perpendicular to the lamellae at a pearlite colony imaged by AFM, and (b) topographic profile of the cementite and ferrite lamellae corresponding to the region crossed by the test-line, for a typical sample of the patented steel (scan speed: 10 µm/s, applied force: 3 nN)

After selecting an image of such a colony, a test-line running perpendicular to the alternating lamellae was applied over the image (Fig. 4a). The image analysis system then provided a topographic profile of the microstructure along the test-line, as shown in Fig. 4(b). The system also offers the possibility of measuring distances between the markers applied to such a profile. Appropriate positioning of these markers allows for the measurement of the distances between the centers of the adjacent cementite or ferrite lamellae. For each selected pearlite colony, it was generally possible to apply three test-lines, leading to an average value of the interlamellar spacing in that colony.

Vickers microhardness (Hv) was measured on metallographically polished steel samples using an applied load of 15 g. The indentation was made on areas A, B, and C, according to Fig. 3. For each area, three measurements were performed, and the average value was determined.

Yield stress was measured by the Instron Universal Testing Machine with special jaws to prevent stress concentration and early wire breakage adjacent to the jaws.

## 3. Results and Discussion

### 3.1 Modeling the Heat Transfer in Air Patenting (Continuous Cooling) and Molten Lead Patenting (Isothermal Cooling)

It can be shown experimentally that the heat flux from the surface of the wire to the surrounding fluid is proportional to the temperature difference between them (Ref 24):

$$q \propto (T_s - T_b) \quad \text{(Eq 1)}$$

where $q$ is the heat flux, $T_s$ is the surface temperature, and $T_b$ is the fluid temperature; or

$$q = h(T_s - T_b) \quad \text{(Eq 2)}$$

The proportionality constant h is defined as the heat transfer coefficient, which is dependant on the thermal diffusivity of the fluid and the properties of the flow system. Its dimensions can be derived from the form of the Eq 2 and are

$$(\text{heat flux})/(\Delta T) \equiv Q/(tTL^2) \quad \text{(Eq 3)}$$

The unit of the heat transfer coefficient is W/m$^2$ K in the SI system.

Two important factors influence the cooling rate: One is the ability of the heat to diffuse from the interior to the surface of the steel specimen, and the other is the ability of the quenching medium to remove the heat from the surface of the part (Ref 25). The heat transfer at the interface of a steel part and a quenching medium is a complex process that depends primarily on the convection currents within the quenching medium that removes the heat from the interface.

Figure 5 shows heat contour at transverse section of wire patenting in air after 10 s (a) and molten lead mediums (b) after 6 s of immersion.

As is expected, heat transfer rate for molten lead medium is much higher than for air, viz., about 40 °C/s for the former compared to only 2.8 °C/s for the latter, because of high convection coefficient (Since, for cooling in air, the temperature decreases from 900 to 872 °C during 10 s, the cooling rate is about 2.8 °C/s. As such, for cooling in lead bath, decreasing from 900 to 501 °C results in a cooling rate of 40 °C/s). This leads to an increased cooling rate and subsequent enhancement of increases in nucleation rate, resulting in a finer pearlite

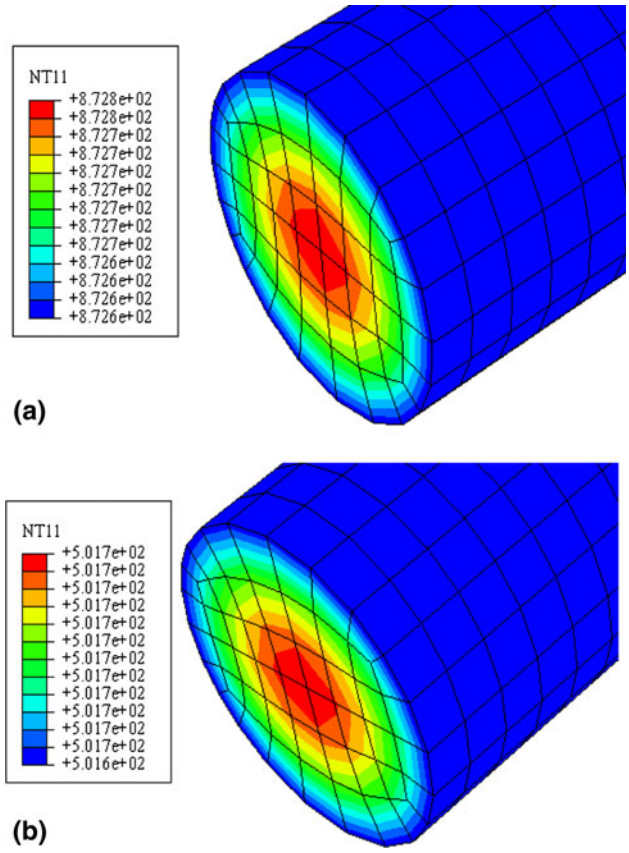


**Fig. 5** Temperature gradient during cooling in (a) air, and (b) molten lead, after 10 s

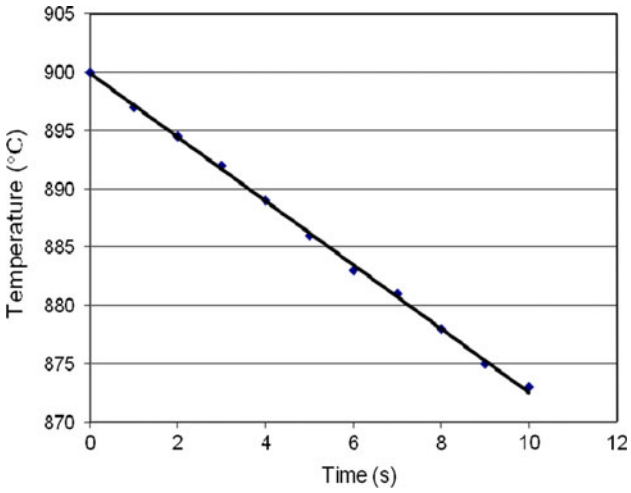


**Fig. 6** Surface temperature of wire during cooling in the air as a function of time

laminar (Ref 25). Therefore, lead patenting is preferred because of the excellent heat transfer properties of the molten lead and its ability to produce a structure with finer interlamellar spacing.

Figures 6 and 7 show the temperature variation at the wire surface as a function of time for air and molten lead medium, respectively.

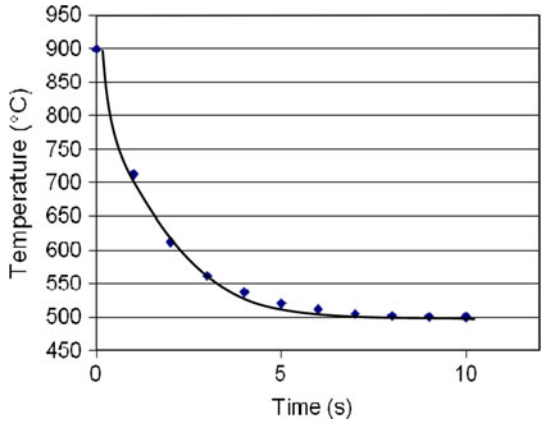


**Fig. 7** Surface temperature of wire during cooling in the lead bath as a function of time

As depicted in Fig. 6, there is a linear decrease of the temperature with time, which can be expressed as

$$T = -2.7318t + 900 \quad \text{(Eq 4)}$$

where $T$ is the surface temperature (°C), and $t$ is the time (s).

According to Fig. 7, there is a nonlinear decrease in temperature with time, and the temperature drops rapidly to that of molten lead temperature within 5 s. Experimental observation shows that the transformation of austenite to pearlite in the quenching step typically takes about 4 s to complete (Ref 26). Therefore, the suitable time for immersion of wire in the lead bath is about 10 s which is in agreement with previous literature (Ref 1).

Obviously, the cooling rate at the surface is higher than that at the center of the wire. Therefore, a temperature gradient forms along the transverse section of the wire. Thermal stress can be calculated by the following equation:

$$S = \alpha E \, \Delta T \quad \text{(Eq 5)}$$

where $S$ is the thermal stress, $\alpha$ is the linear expansion coefficient, $E$ is the elastic modulus, and $\Delta T$ is the temperature difference between the surface and the center.

As shown in Fig. 5, for example, after 10 s, the temperature difference between surface and center is very low (surface temperature is very close to center temperature). That is, the thermal stress owing to the temperature difference is negligible.

### 3.2 Relationship Between Undercooling and Interlamellar Spacing

For constant austenitizing temperature (910 °C), the resulting interlamellar spacing is plotted as a function of the inverse of the undercooling (Fig. 8). The corresponding standard deviation error is about ±4% of the measured amounts. This error arises from insignificant difference in interlamellar spacing in different regions of sample (Fig. 3).

It is observed that the interlamellar spacing decreases with decreasing transformation temperature which is in agreement with other investigations (Ref 12, 21). The dependence of the interlamellar spacing on the transformation conditions is linked to the change in the growth rate. As the transformation temperature increases or the undercooling decreases; the

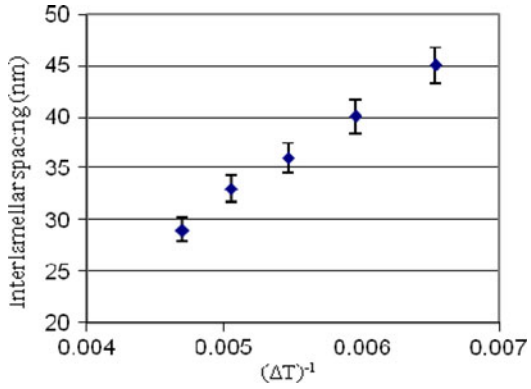


**Fig. 8** Interlamellar spacing as a function of inverse of under cooling for constant austenitizing temperature or 910 °C

driving force for transformation decreases. Moreover, at lower temperatures, the lower diffusivity of carbon atom reduces the diffusion distance, and as a consequence, reduces the pearlite interlamellar spacing (Ref 27).

From Fig. 8, it is apparent that the interlamellar spacing follows a linear relationship with the inverse amount of undercooling; this can be represented by the best fit equation as follows:

$$S = 6450 * (\Delta T)^{-1} \quad \text{(Eq 6)}$$

where $S$ is the interlamellar spacing (nm), and $\Delta T$ is the undercooling below $A_{e1}$.

The interlamellar spacing was first measured systematically for a number of steels by Mehl et al. (Ref 28), who demonstrated that the spacing decreases by increasing the undercooling, $\Delta T$, below the eutectoid temperature. Therefore, the minimum interlamellar spacing was obtained for quenching temperature of 510 °C (Fig. 8). According to Krauss (Ref 25), many relationships for the change in interlamellar spacing with undercooling have been proposed, but the best one was developed by Zener and Hillert. The relation was derived purely on thermodynamic grounds. The formation of volume of pearlite causes an increase in interfacial energy by virtue of the new ferrite and cementite interfaces formed. They assumed that growth of the lamellae can only occur if the increase in surface energy is less than the decrease in energy resulting from the transformation. They predicted that the system stabilizes at a spacing for which the growth rate is a maximum and this criterion leads to (Ref 29)

$$S = (4\sigma_{\alpha/Fe_3C} T_E)/(\Delta H_V \Delta T) \quad \text{(Eq 7)}$$

where $\sigma_{\alpha/Fe_3C}$ is the interfacial energy per unit area of $\alpha/Fe_3C$ boundary, $T_E$ is the equilibrium temperature in K ($A_{e1}$ in the case of Fe-C alloys and steels), and $\Delta H_V$ is the change in enthalpy per unit volume between austenite and the mixture of ferrite and cementite.

According to Eq 6 and 7

$$(4\sigma_{\alpha/Fe_3C} T_E)/\Delta H_V = 6450 \quad \text{(Eq 8)}$$

and $T_E = 996$ (K), $\Delta H_V = 6.09 \times 10^{-19}$ J/nm$^3$ (Ref 30). Therefore, $\sigma_{\alpha/Fe_3C} = 0.98 \times 10^{-18}$ J/nm$^2$.

These are in good agreement with the reported values in the literature (Ref 31).

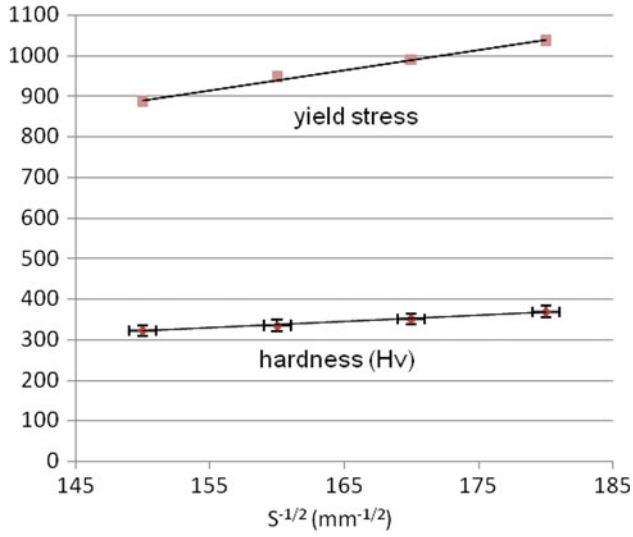


**Fig. 9** Hardness and yield stress as a function of the inverse of the square root of the interlamellar spacing

### 3.3 Relationship Between Hardness and Yield Stress, and the Interlamellar Spacing

The yield stress of high carbon steels is controlled by the pearlite interlamellar spacing (Ref 32). It is well established that the yield stress increases as the interlamellar spacing decreases (Ref 33, 34). This behavior may be attributed to the difficulty in the dislocation motion, to the short slip distance during the plastic deformation of fine pearlite, as well as to the presence of the discontinuous proeutectoid, ferrite (Ref 35).

The hardness and yield strength of the steel wire are plotted as a function of the inverse amount of the square root of the interlamellar spacing ($S^{-1/2}$) in Fig. 9. For hardness results, the corresponding standard deviation error is about ±4% of the measured amounts. This error may be arising from insignificant difference in interlamellar spacing in different regions of the sample (Fig. 3). Hardness and yield strength of the steel wire follow a linear relationship with $S^{-1/2}$ (Fig. 9). This is in line with some previous studies (Ref 18-20) and in contrast with the results of some others (Ref 22, 23) which are in favor of rather inverse relationship between yield stress and interlamellar spacing (i.e., $\sigma_{ys} = \sigma_0 + K_y S^{-1}$). Assuming (Ref 11)

$$\text{Hv} = H_0 + K_H S^{-1/2} \quad \text{(Eq 9)}$$

$$\sigma_{ys} = \sigma_0 + K_y S^{-1/2} \quad \text{(Eq 10)}$$

where Hv is the Vickers hardness, $H_0$ is the hardness of the ferrite with infinite mean free path, $K_H$ is related to the dislocation locking constant during hardness measurement, $\sigma_{ys}$ the yield strength of the steel, $\sigma_0$ the internal frictional strength of ferrite with infinite mean free path which equals to: $\sigma_0 = \sigma_i + \sigma_s + \sigma_{pn} + \sigma_d + \sigma_{ss} + \sigma_t$, where the subscripts i, s, pn, d, ss, and t represent the contributions from internal stress, solid solution, precipitation, dislocation density, substructure and texture, respectively. $K_y$ is the dislocation locking constant during yielding.

Given the amount of intercepts and slopes (Fig. 9), the following relationships were obtained:

$$H = 1.54 S^{-1/2} + 89.4 \quad \text{(Eq 11)}$$

$$\sigma_{ys} = 4.92S^{-1/2} + 151.7 \quad \text{(Eq 12)}$$

According to Eq 9 and 10, the obtained amounts for hardness and yield stress of ferrite (i.e., $H_0$, $\sigma_0$) are in agreement with experimental results (The hardness of ferrite is less than 100 (HV), and the yield stress of ferrite is less than 200 (MPa)).

To verify the validity of the inverse relation between yield stress and interlamellar spacing, one may assume

$$\text{Hv} = H_0 + K_H S^{-1} \quad \text{(Eq 13)}$$

$$\sigma_{ys} = \sigma_0 + K_y S^{-1} \quad \text{(Eq 14)}$$

Given the obtained results for the steel wire studied in this study: $\sigma_0$ = 505.68 (MPa), and $H_0$ = 198 (HV).

Based on the discrepancy between the results obtained from Eq 13 and 14 and the experimental results, the linear relationship between the inverse amount of the square root of the interlamellar spacing ($S^{-1/2}$) and yield stress is justified.

### 3.4 Effect of the Amount of Prior Deformation on the Resulted Interlamellar Spacing After Patenting

To study the effect of the prior deformation on the resultant interlamellar spacing, patenting treatment was carried out on the wires with different previous percent values of area reductions under similar austenitizing and quenching temperature (Table 2).

Apparently, the wire with the higher reduction of area (i.e., 1.8 mm diameter) has the lowest interlamellar spacing. Therefore, it seems that by increasing the prior deformation, the amount of interlamellar spacing after patenting treatment decreases. This can be explained in terms of pearlite transformation characteristics where austenite formation is very much a function of the starting microstructure. In pearlitic structures, austenitization may be regarded as a reverse reaction of eutectoid transformation:

$$\alpha(0.002\%\ \text{C}) + \text{Fe}_3\text{C}(6.67\%\ \text{C}) = \gamma(0.77\%\ \text{C}) \quad \text{(Eq 15)}$$

The above equation shows that considerable diffusion of carbon is necessary for austenite formation to balance the carbon in the cooperating phases. Cementite is the source of carbon for the austenite, and therefore, the reaction begins at the carbon-rich ferrite/cementite interface. The nucleation of the austenite takes place preferentially at the points of intersection of cementite with the edges of the pearlite colony and at the ferrite/cementite interface within a pearlite colony (Fig. 10) (Ref 36).

As drawing strain increases, the interlamellar spacing decreases (Ref 37). On the other hand, lower pearlite interlamellar spacing induces higher number of austenite nucleation because of the increase in preferential nucleation sites (Ref 38). Therefore, with increasing number of austenite nuclei, the grain size of the resultant austenite decreases, leading to increasing austenite grain boundary. Referring to Elwazri et al. (Ref 39), austenite grain size directly affects the resultant interlamellar spacing. The influence of the prior austenite grain size on pearlite interlamellar spacing was reasoned previously on the basis of the total grain boundary area, which increases as the grain size decreases on account of an increase in the nucleation sites for ferrite and cementite phases (Ref 11).

**Table 2 Characteristics of the used wires**

| Diameter, mm | Reduction of area, % |
|---|---|
| 1.8 | 89 |
| 2 | 87 |
| 2.7 | 86 |
| 3.2 | 84 |

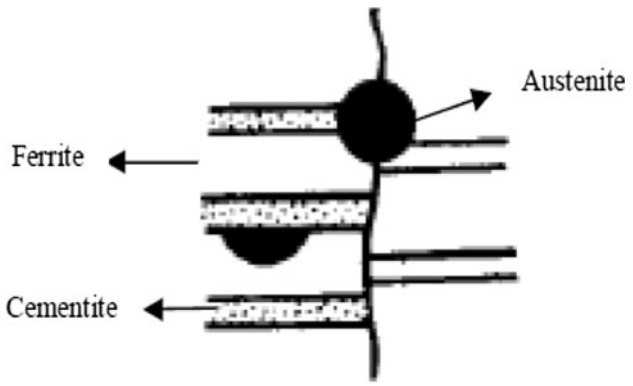


**Fig. 10** Nucleation sites for austenite formation in microstructure of pearlite (Ref 25)

## 4. Conclusions

1. The model presented in this study enables us to predict the immersion time for hypoeutectoid steel wire in the lead bath. The suitable immersion time for the wire with 1.8-mm diameter is about 10 s.
2. Austenitizing and quenching temperatures for a wire with 1.8-mm diameter and 0.72% C to obtain the lowest interlamellar spacing (i.e., 29 nm) are 910 and 510 °C, respectively.
3. Hardness and yield strength of the steel studied follow a linear relationship with the inverse amount of the square root of the interlamellar spacing ($S^{-1/2}$).
4. Pearlite interlamellar spacing obtained after patenting treatment decreases by increasing the amount of prior deformation.


## Acknowledgment

The authors would like to thank Mahar Fan Abzar (MFA) Company for providing AFM for the research study.


## References


1. J.E. Swindells and R. Monavo, *Ferrous Wire Handbook*, revised ed., R.M. Shemenski, Ed., Wire Association International, Guilford, USA, 2008, p 1162
2. J. Horsfall, Manufacture of Wire Rope, B. Patent, 1856
3. M.G. Zelin, T.W. Starinshak, and J. Terry, High Strength, High Carbon Steel Wire, The Goodyear Tire & Rubber Company, US Patent 6949149, 2005
4. M. Munirajulu, B.K. Dhindaw, and A. Biswas, Modeling of Eutectoid Transformation in Plain Carbon Steel, *ISIJ Int.*, 1994, **34**, p 355–358
5. C. Zener, Kinetics of the Decomposition of Austenite, *Trans. AIME*, 1946, **167**, p 550–583

6. F.G. Caballero, C. Capdevila, and C.G. de Andres, Influence of Pearlite Morphology and Heating Rate on the Kinetics of Continuously Heated Austenite Formation in a Eutectoid Steel, *Metall. Mater. Trans. A*, 2001, **32A**, p 1283–1291
7. F.G. Caballero, C. Capdevila, and C.G. de Andres, Modeling of Kinetics of Austenite Formation in Steels, *ISIJ Int.*, 2001, **41**, p 1093–1102
8. N. Ridley, A Review of the Data on the Interlamellar Spacing of Pearlite, *Metall. Trans.*, 1984, **16A**, p 1019–1036
9. J. Aghazadeh, Effect of Tungsten on the Pearlite Reaction in a Eutectoid Steel, *J. Eng., Islamic Republic of Iran*, 1995, **8**, p 147–157
10. V.T.L. Buono, B.M. Gonzalez, and T.M. Lima, Measurement of Fine Pearlite Interlamellar Spacing by Atomic Force Microscopy, *J. Mater. Sci.*, 1997, **32**, p 1005–1008
11. O.P. Modi, N. Deshmukh, and D.P. Mondal, Effect of Interlamellar Spacing on the Mechanical Properties of 0.65% C Steel, *Mater. Charact.*, 2001, **46**, p 347–352
12. T. Gladman and F. Pickering, *Yield, Flow and Fracture of Polycrystals*, T.N. Baker, Ed., Applied Science Publisher, London, UK, 1983
13. P.-H. Chang and A. Preban, The Effect of Ferrite Grain Size Martensite Volume Fraction on the Tensile Properties of Dual Phase Steel, *Acta Metall.*, 1985, **33**, p 893–903
14. D. Mondal, K. Ray, and S. Das, The Strength of Ferrite in Annealed Armco Iron and Hypoeutectoid Steels, *Z. Metallkd.*, 1998, **89**, p 635–641
15. J. Baird, Effect of Subgrain Size on the Flow Stress of Iron, *J. Iron Steel Inst.*, 1966, **204**, p 44–45
16. N. Petch, The Ductile Brittle Transition in Structure of α-Iron, *Philos. Mag.*, 1958, **3**, p 1089–1097
17. A. Marder and B. Bramfitt, The Effect of Morphology on the Strength of Pearlite, *Metall. Trans.*, 1976, **7A**, p 365–372
18. J. Sevillano, On the Yield and Flow Stress of Lamellar Pearlite, *Proceedings of ICSMA-5* (Oxford, UK), Pergamon, 1979
19. K. Ray and D. Mondal, The Strength of Pearlite in Annealed Eutectoid and Hypoeutectoid Steel, *Acta Metall. Mater.*, 1991, **39**, p 2201–2206
20. L. Brown and R. Ham, *Strengthening Methods in Crystals*, Applied Science Publication, London, UK, 1971
21. A.M. Elwazri, P. Wanjara, and S. Yue, Measurement of Pearlite Interlamellar Spacing in Hypereutectoid Steels, *Mater. Charact.*, 2005, **54**, p 473–478
22. J.M. Hyzak and I.M. Bernstein, The Role of Microstructure on the Strength and Toughness of Fully Pearlitic Steels, *Met. Trans.*, 1976, **7A**, p 1217–1224
23. A.R. Marder and B.L. Bramfitt, The Effect of Morphology on the Strength of Pearlite, *Met. Trans.*, 1976, **7A**, p 365–372
24. N.J. Themelis, *Transport and Chemical Rate Pheomena*, Gardon and Bread Publisher, 1995, p 369
25. G. Krauss, *Steels, Processing, Structure and Performance*, The University of Michigan, 2005, p 613
26. A.W. Bhagwat and E.F. Riggenbach, *Process for Patenting and Brass Plating Steel Wire*, The Goodyear Tire & Rubber, US Patent 5437748, 1995
27. R.W.K. Honeycombe and H.K.D.H. Bhadeshia, *Steels Microstructure and Properties*, Edward Arnold, London, 1995
28. R.F. Mehl, C.S. Barrett, and D.W. Smith, Studies Upon the Widmanstatten Structure, *Trans. AIME*, 1933, **105**, p 215–258
29. M.P. Puls and J.S. Kirkaldy, The Pearlite Reaction, *Metall. Trans. A*, 1972, **3**, p 2777–2796
30. C. Capdevila, F.G. Caballero, and C.G.D. Andres, Neural Network Model for Isothermal Pearlite Transformation, *ISIJ Int.*, 2005, **45**, p 229–237
31. S.E. Offerman, L.J.G.W. van Wilderen, and N.H. van Dijk, In Situ Study of Pearlite Nucleation and Growth During Isothermal Austenite Decomposition in Nearly Eutectoid Steel, *Acta Mater.*, 2003, **51**, p 3927–3938
32. W.C. Leslie, *The Physical Metallurgy of Steels*, McGraw-Hill, 1982, p 396
33. E.M. Taleff, Pearlite in Ultrahigh Carbon Steels: Heat Treatments and Mechanical Properties, *Metall. Mater. Trans. A*, 1996, **27A**, p 111–118
34. D.J. Alexander and I.M. Bernstein, Microstructural Control Flow and Fracture in Pearlitic Steels, *Metall. Trans. A*, 1987, **20A**, p 2321–2335
35. W. Smith, *Structure and Properties of Engineering Alloys*, McGraw-Hill, 1981, p 512
36. G.R. Speich and A. Szirmae, Formation of Austenite from Ferrite and Ferrite-Carbide Aggregates, *Trans. TMS-AIME*, 1969, **245**, p 1063–1074
37. Y.S. Yang, J.G. Bae, and C.G. Park, Nanostructure and Mechanical Properties of Heavily Cold-Drawn Steel Wires, *Mater. Sci. Eng. A*, 2009, **508**, p 148–155
38. F.G. Caballero, C. Capdevila, and C.G. de Andre's, Influence of Scale Parameters of Pearlite on the Kinetics of Anisothermal Pearlite to Austenite Transformation in a Eutectoid Steel, *Scripta Mater.*, 2000, **42**, p 1159–1165
39. A.M. Elwazri, P. Wanjara, and S. Yue, The Effect of Microstructural Characteristics of Pearlite on the Mechanical Properties of Hypereutectoid Steel, *Mater. Sci. Eng. A*, 2005, **404**, p 91–98